Egyptian Geophysical Society
EGS Journal, Vol. 13, No. 1, 57-66 (2015)

AIRBORNE MAGNETIC DATA INTERPRETATION OF AL-AYS SEISMICALLY ACTIVE AREA, SAUDI ARABIA

E. Elawadi[1, 2]

(1) King Saud University, Riyadh, KSA 11451, E-mail eelawadi@ksu.edu.sa
(2) Nuclear Materials Authority, P.O. Box 530 El- Maadi, Cairo, Egypt.

تفسير البيانات المغناطيسية الجوية فى منطقة العيص ذات النشاط الزلزالى بالمملكة العربية السعودية

الخلاصة: تفسير البيانات المغناطيسية للمناطق النشطة زلزاليا وبركانيا يمكن أن يوفر معلومات قيمة تساعد على تصور السيناريو الأكثر احتمالا للوضع الزلزالى للموقع وتوقع النشاط فى المستقبل. رسم الوضع التركيبى للمنطقة يسمح بتوضيح طبيعة الأنشطة الزلزالية والتراكيب المرتبطة بها . علاوة على ذلك، تكرار القياسات المغناطيسية للمواقع النشطة زلزاليا يوفر معلومات عن تطور النشاط البركانى وحركة الصخور المنصهرة تحت السطح . تقدم هذه الدراسة تحليلاً وتفسيراً للبيانات المغناطيسية لمنطقة العيص، غرب المملكة العربية السعودية. النشاط الزلزالى لهذه المنطقة بدأ منذ العصر السينوزوى (مع تكزين إخدود البحر الأحمر) و مؤخرا سجل نشاط زلزالى بالمنطقة بلغ أقصاه بزلزال شدته ٥,٧ درجة تلاها عشرات الآلاف من الزلازل الصغيرة .تحليل البيانات المغناطيسية يمكننا من تعيين أعماق وإمتدادات التدفقات البازلتية، والعمق إلى درجة حرارة الإنصهار للصخور (نقطة كورى) ويوفر معلومات أساسية عن القياسات المغناطيسية المستقبلية لرصد تحركات الماجما من ناحية أخرى، وإن تفسير التراكيب الجيولوجية القريبة من السطح والعميقة يظهر الارتباط المكانى للزلازل المتوسطة (أكثر من ٤ درجات) مع إتجاه التراكيب شمال شمال الغرب–جنوب جنوب الشرق فى حين أن الزلازل الصغيرة ترتبط بالتراكيب ذات شمال شرق–جنوب غرب وشمال شمال الغرب–جنوب جنوب الشرق.

ABSTRACT: *Interpretation of magnetic data for the volcanic and seismic active areas can provide valuable information required to imagine the most likely scenario of the site situation and future activity. Mapping the structural architecture allows elucidating the nature of the seismic activities and the controlling structures. Moreover, repeated magnetic measurements provide a key tool to update the state of the volcanic activity and magmatic intrusions. This study presents the analysis and interpretation of the magnetic data of Al-Ays area, western Saudi Arabia. The area has known Cenozoic volcanic eruption and recently possessed an earthquake of 5.7 magnitudes, followed by tens of thousands of small earthquakes. Magnetic data analysis enables mapping the depth and extent of the basaltic flows, the depth to the Curie isotherm (high-temperature magma) and provides baseline information for future magnetic measurements to monitor the magma intrusions. On the other hand, the interpreted near-surface and deep-seated structures shows spatial correlation of the medium earthquakes (more than 4 magnitudes) with the NNW-SSE structural trend while the minor events correlated to both the NE-SW and NNW-SSE structural trend.*

INTRODUCTION

Al-Ays area recently experienced intermediate earthquakes with maximum magnitude of 5.7 followed by a swarm of thousands of earthquakes (Fig. 1). Between April and June 2009, more than 30,000 earthquakes struck an ancient lava field named Harrat Lunayyir, with 19 earthquakes of magnitude 4, or greater, striking at the swarm's peak on May 19. Most of the aftershocks are clustered along two directions (NNW and NE) and located in the top-most crust from 5-10 km depth, as reported by Saudi Geological Survey (SGS) website. The lava field of Harrat Lunayyir is part of a "lava province" roughly 180,000 square kilometers in size that began forming 30 million years ago associated with the Red Sea rifting split of Arabian shield from Africa.

The area is included in the airborne magnetic survey over the Arabian shield conducted between 1965 and 1967 and compiled for the entire shield since 1985. Despite this early magnetic survey and the tectonic activity of this province, few publications addressed the regional analysis and interpretation of the magnetic data of the whole shield (Nehling et al., 2002) and selected areas (Mashael, 2008, Elawadi et al., 2012, and Elawadi et al., 2013).

This study presents the analysis and interpretation of the airborne magnetic data of the area with a primary aim to support elucidating the nature of the seismic activities and provide baseline information to update the state of the volcanic activity and magmatic intrusions. Mapping subsurface geologic units and structures provides essential information for seismic hazards and risk assessment studies as well.

REGIONAL GEOLOGY

Generally, the area can be divided into two main geological units (Fig. 2), the Precambrian basement rocks and the Cenozoic basaltic extrusive rocks.

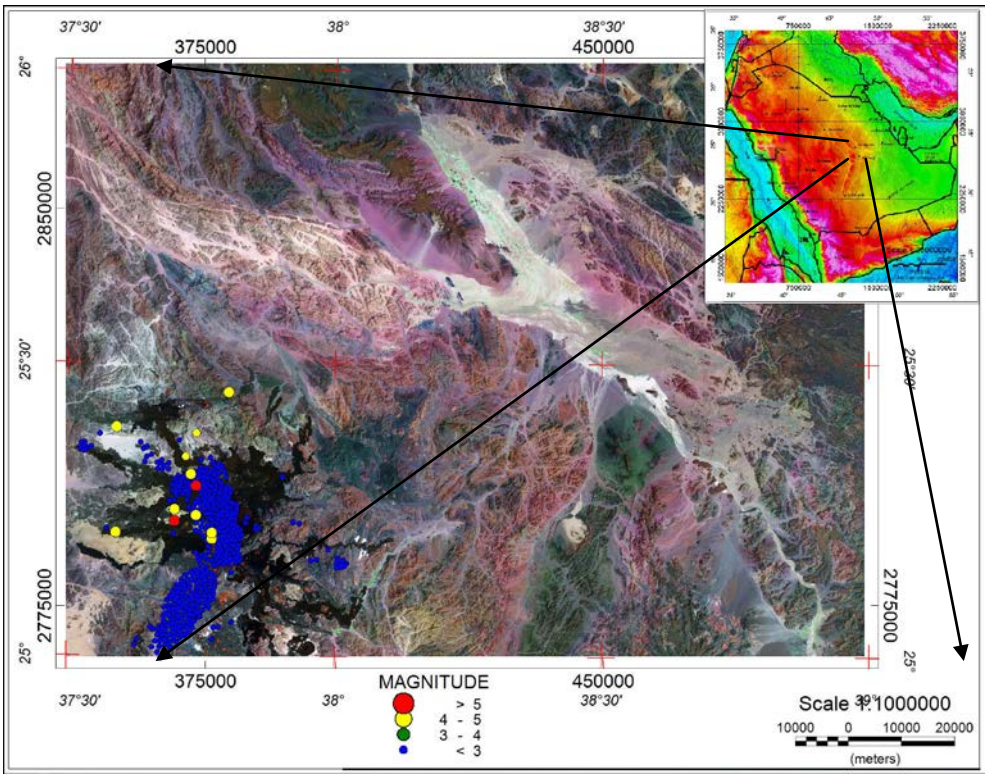

Fig. (1): Location and satellite image of the study area. Colored circles present the locations and magnitudes of the recent earthquake events.

Precambrian rocks (570-690 Ma), covering most of the area, are represented from the oldest by undifferentiated schist and gneiss, Farri group (volcanic rocks such as andesite and rhyolite, welded tuff, pillow lava, serpentinite and gabbro), Al-Ays group (breccia, conglomerate and basalt) and Hadiyah group (sandstone, basalt, diorite and pillow lava). Among these rocks granite and gabbro rocks had been formed as injected magma representing big mountains and ring-like bodies located at different locations of the area.

Tertiary (0.3 to 25 Ma) and Quaternary (recent to 0.3 Ma) volcanic rocks including Harrat Lunayyir and Harrat Khaybar consists of basalt and andesite and are located directly above the older, Precambrian, basement rocks in the south western and middle eastern parts of the study area. Tectonically, the area was subjected to two episodes of tectonic movements synchronized with the Red Sea floor spreading through pre-early Miocene rifting period (Anon, 1972; Rose et al., 1973). It has been controlled-to great extent-by the regional stress regime of the western Arabian plate associated with the Cenozoic development of the Red Sea. The seismically active area (Harrat Lunayyir) probably faulted during Cenozoic rift time where the up arching period was parallel to the Red Sea coast. The geologic map of the area (Fig. 1) shows a series of synclinal and anticlinal folds trending mainly in NW-SE and faults of different directions, WNW-ESE (Najd trend), E-W (Tethyan trend), ENE-WSW (Syrian Arc trend), and NW-SE (Red sea trend).

The seismically active (Harrat Lunayyir) area is affected by different fault systems oriented NE-SW, NNW-SSE, and NW-SE. The alkali basalt invaded into the Harrat Lunayyir during Late Miocene-Pliocene. Modelling of Interferometric Synthetic Aperture Radar (InSAR) data, carried out by SGS after the 2009 earthquaqe, indicates that close to 40 cm of regional uplift and well over 1 meter of east-west extension occurred. The earthquakes and ground deformation resulted from tensional faulting that is consistent with intrusion of a 2 m thick magmatic dike of about 0.13 km^3 volume, with its top at less than 2 km depth. The faulting is consistent with previous observations that the Quaternary volcanism has been concentrated along an orientation about N35^{o}W (SGS webpage and Pallister et al., 2010).

DATA ANALYSIS AND INTERPRETATION

Two analysis techniques were applied to the R.T.P magnetic data (Fig. 3) as a guide for structural interpretation. These methods are Euler deconvolution (Thompson, 1982; and Reid et al., 1990), and local wave number (Thurston and Smith 1997; Smith and Thurston, 1998).

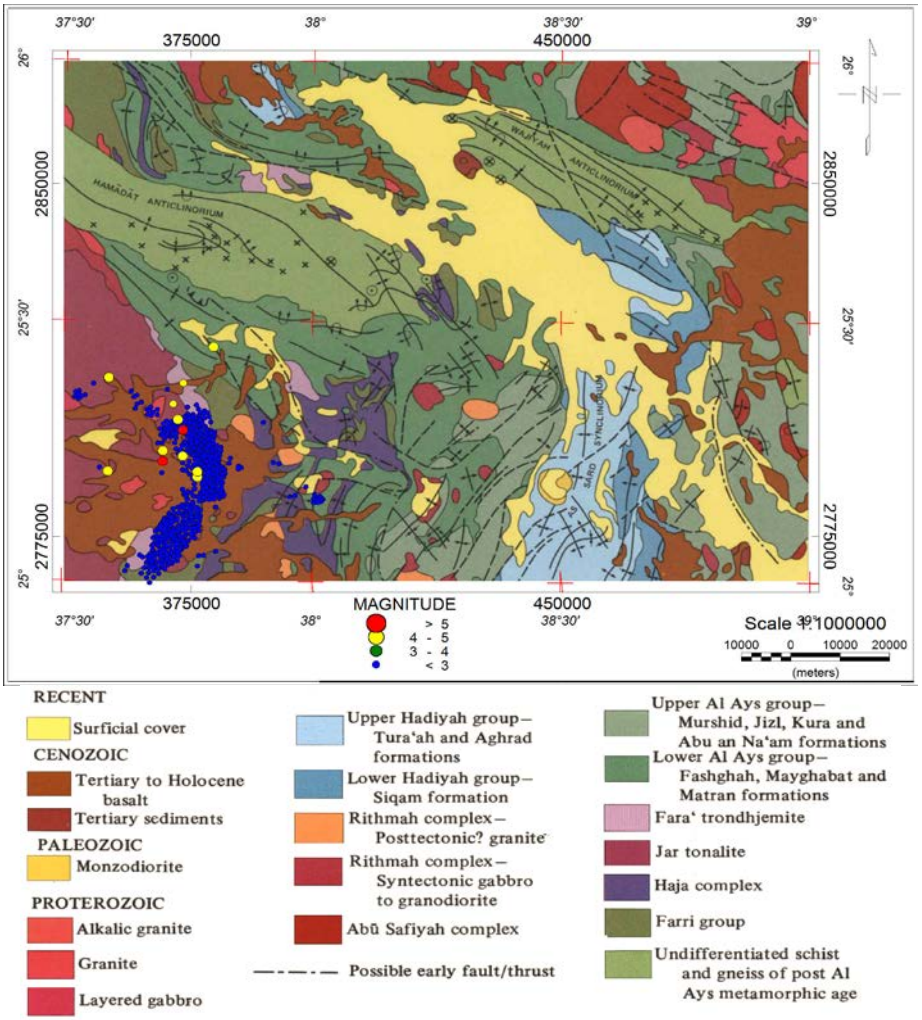

Fig. (2): Simplified geologic map of the study area (compiled by Kemp, 1981). Colored circles present the locations and magnitudes of the recent earthquake events.

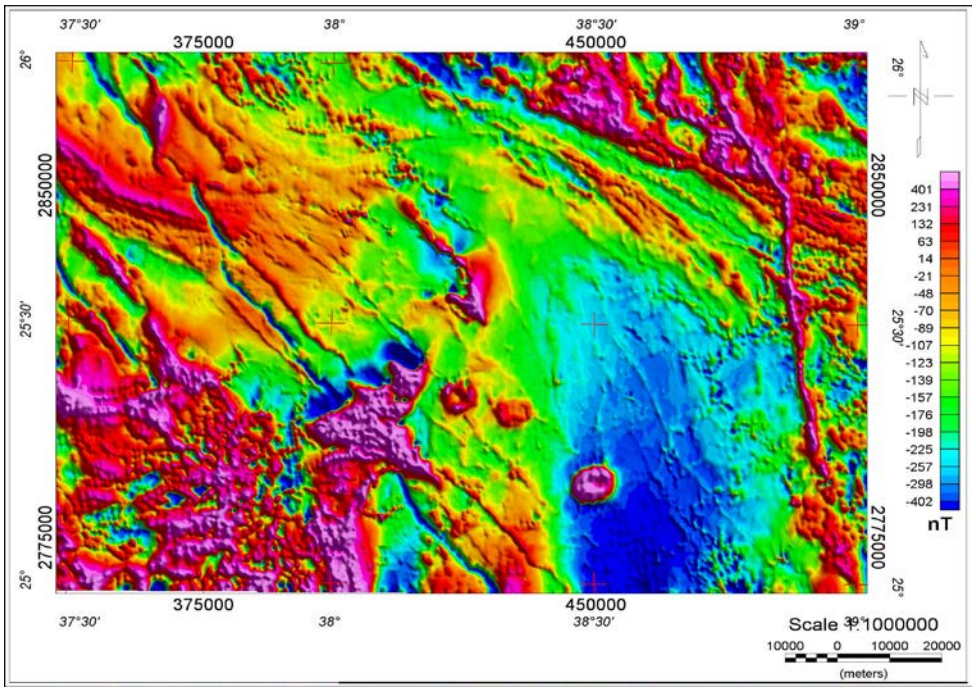

Fig. (3): R.T.P Total magnetic intensity map of the area.

These methods are proven as efficient tools to map the location and depth of magnetic structures such as faults and contacts. To improve the signal-to-noise ratio of the data prior to application of these methods, filtering technique was applied to separate the regional and residual magnetic components and remove the noise. Filtering and derivatives were applied to the gridded magnetic data in the frequency domain using Geosoft software package (Geosoft, 2005).

Filtering the magnetic data:

The objective of the filter is to condition the data set and to render the resulting presentation in such a way as to make it is easier to interpret the significance of anomalies in terms of their geological sources (Bird, 1997). Therefore, the most effective way to filter the data is with an understanding of the geologic control and the desired filtered results. Several filtering techniques can be performed in the frequency domain. However, one of the most traditional filters, used in the potential field, is the separation of long (deep) and short (shallow) wavelength anomalies. The success of this technique depends on the proper choice of cut-off wavelength used in the filter design. The cut-off wavelengths and information about the contribution of the short and long wavelengths in the spectrum can be obtained from the calculated radially-averaged power spectrum of the data.

Two-dimensional power spectrum curve of the present RTP data (Fig. 3) shows two linear segments related to long and short wavelength components with frequency bands ranges from 0.0 to 0.042 and from 0.04 to 0.4 wavenumbers, respectively (Fig. 4). Following Spector and Grant (1970), the slope of these two linear segments were used to estimate the average depth (≈6.0 and ≈1.5 km) to the top of the deep-seated and near-surface magnetic sources, respectively. These depths are average estimates for the entire area and do not reflect a resolved and quantitative topography of the basement surface. The frequency bands corresponding to these linear segments were used through the Butterworth filter technique to produce the regional and residual magnetic component maps.

To enhance mapping of the basaltic flow and near-surface intrusions, further horizontal derivative and analytic signal were applied to the residual map to produce the enhanced residual map (Fig. 5). This map shows that the basaltic flow in the southwestern part at the subsurface is wider than that mapped at the surface geoloic map. Moreover, similar magnetic signature indicating near-surface volcanic intrusins can obvoiusely mapped in the northern and norteastern zones of the study area in fair agreement with the mapped geology. This map enhansed, on the other hand, the signature of the dikes intruded in the area and trending mainly in NNW-SSE direction. Zones of cold colours indicte absence of magnetic sources at near-surface level.

Euler deconvolution:

Euler deconvolution is an automatic technique used for locating the source of potential field based on both their amplitudes and gradients. The method was developed by Thompson (1982) to interpret 2D magnetic anomalies and extended by Reid et al. (1990) to be used on grid-based data. Magnetic field M and its spatial derivatives satisfy Euler's equation of homogeneity.

$$(x-x_\circ)\frac{\partial M}{\partial x}+(y-y_\circ)\frac{\partial M}{\partial y}+(z-z_\circ)\frac{\partial M}{\partial z}=-NM, \qquad (1)$$

where $\partial M/\partial x$, $\partial M/\partial y$ and $\partial M/\partial z$ represent first-order derivative of the magnetic field along the x-, y- and z-directions, respectively, N is known as a structural index and related to the geometry of the magnetic source. For example, N=3 for sphere, N=2 for pipe, N=1 for thin dike and N=0 for magnetic contact (Reid et al., 1990). Taking into account a base level for the regional magnetic field (B), equation (1) can be rearranged and written as

$$\mathrm{x}_\circ\frac{\partial \mathrm{M}}{\partial \mathrm{x}}+\mathrm{y}_\circ\frac{\partial \mathrm{M}}{\partial \mathrm{y}}+\mathrm{z}_\circ\frac{\partial \mathrm{M}}{\partial \mathrm{z}}+\mathrm{NB}=$$

$$\mathrm{x}\frac{\partial \mathrm{M}}{\partial \mathrm{x}}+\mathrm{y}\frac{\partial \mathrm{M}}{\partial \mathrm{y}}+\mathrm{z}\frac{\partial \mathrm{M}}{\partial \mathrm{z}}+\mathrm{NM.}, \qquad (2)$$

Assigning the structural index (N), a system of linear equations can be obtained and solved for estimating the location and depth of the magnetic body. Using a moving window, multiple solutions from the same source can be obtained. Good solutions are considered to be those that cluster well and have small standard deviations (Thompson 1982; Reid et al., 1990). Euler solutions were filtered using the criteria of Reid et al. (1990) to remove the solutions of low certainty. Filtered solutions are plotted over a background of the magnetic components. The method was applied to the filtered regional and residual magnetic component maps to provide depth and location of the magnetic source bodies. For the regional map the structure index of (N=0) was assigned to map the deep-seated magnetic contacts (Fig. 6), while the structure index of (N=1) was assigned to the residual magnetic map to render the dike bodies predominant in the near-surface (Fig. 7).

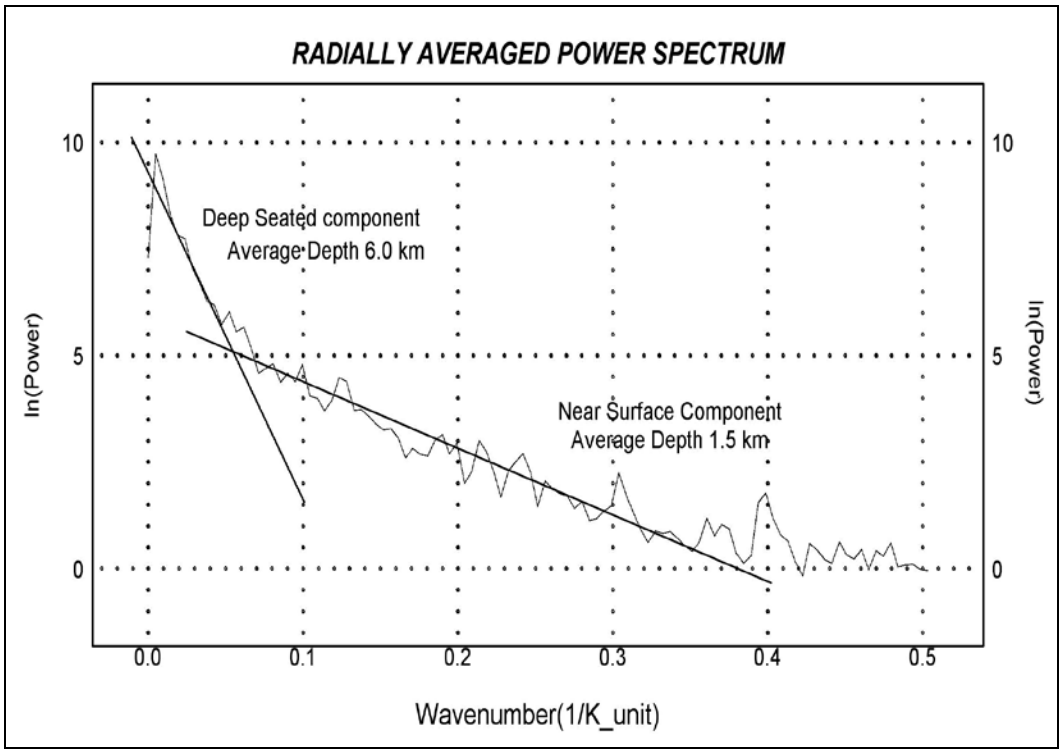

Fig. (4): Power spectrum of the RTP magnetic map (Fig. 3).

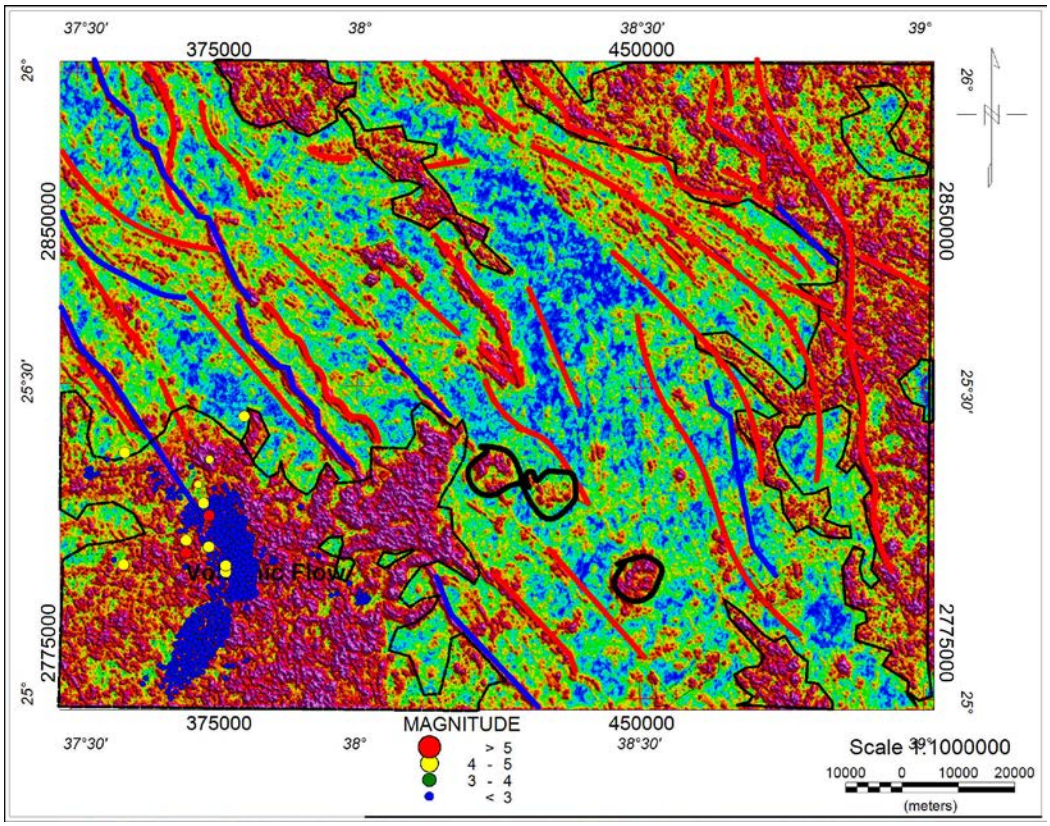

Fig. (5): Enhanced residual magnetic map overlaid by the interpreted near-surface basaltic flow zones (polygons), acidic (red lines) and basic (blue lines) dikes and ring-like intrusions.

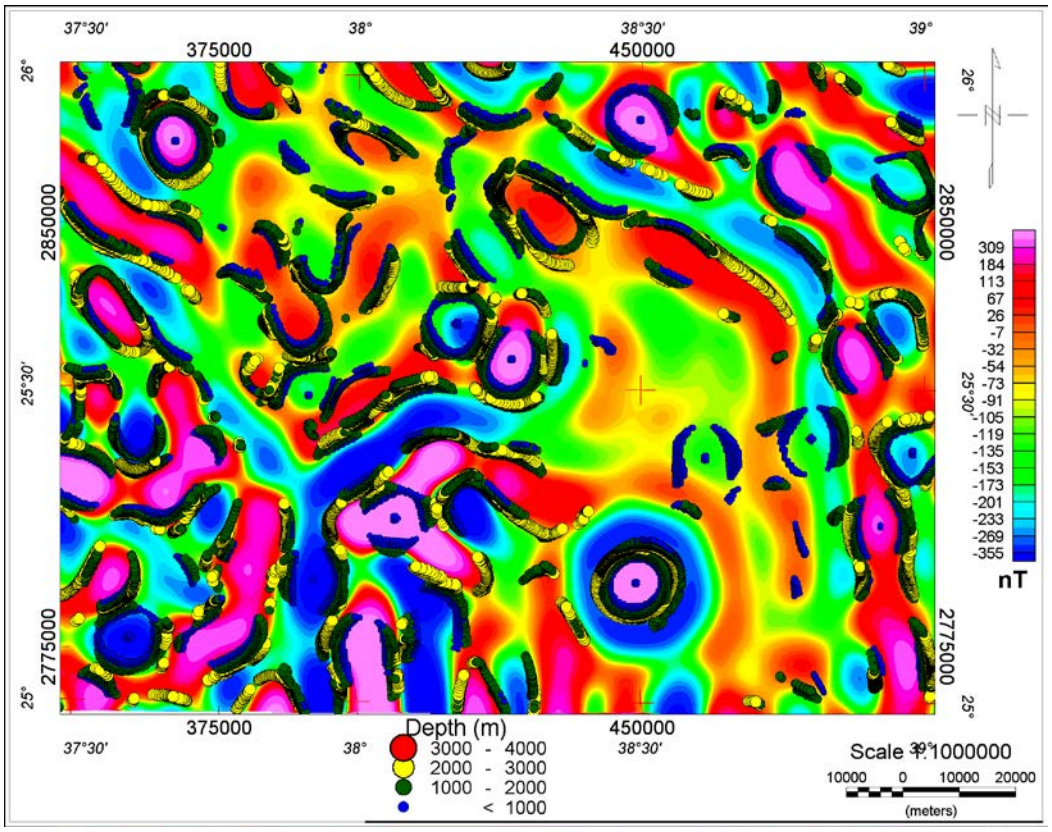

Fig. (6): Euler solutions of the regional magnetic component map assigning structural index of contact (N=0) displayed over the second vertical derivative SVD of the regional map.

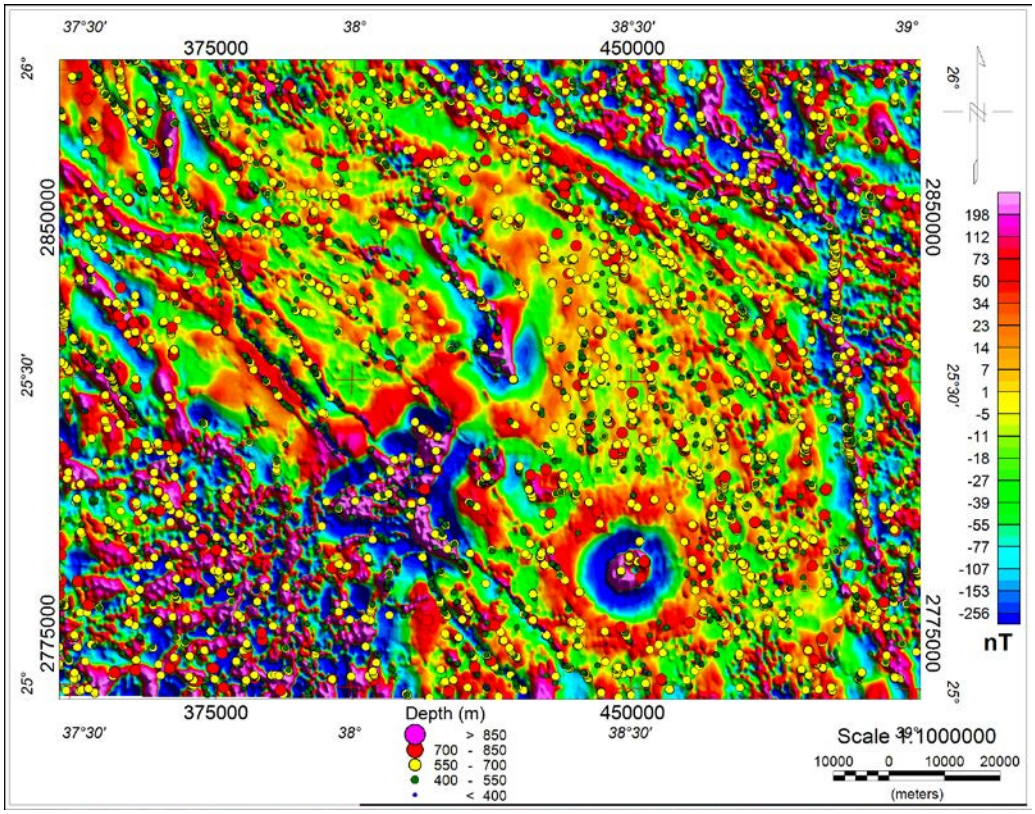

Fig. (7): Euler solutions of the residual magnetic component map (inset as background) assigning structural index of dike (N=1).

Generally, the Euler solutions (Figs. 6 and 7) show good clustering along linear segments trending commonly in NW, NNW, and NE directions. Moreover, the Euler solutions provide depth estimation to the deep-seated contacts range from 400m to 2900m and from 225 to 740m for the near-surface dikes.

Local wavenumber (SPI) method:

Local wavenumber is a technique based on the extension of complex analytical signal to estimate magnetic depths. The original SPI method (Smith et al., 1998) works for two models: a 2-D sloping contact or a 2-D dipping thin-sheet. For the magnetic field M, the local wavenumber (Smith et al., 1998) is given by

$$k = \frac{\frac{\partial^2 M}{\partial x \partial z}\frac{\partial M}{\partial x} - \frac{\partial^2 M}{\partial x^2}\frac{\partial M}{\partial z}}{\left(\frac{\partial M}{\partial x}\right)^2 + \left(\frac{\partial M}{\partial z}\right)^2} \qquad (3)$$

For the dipping contact, the maxima of k are located directly over the isolated contact edges and are independent of the magnetic inclination, declination, dip, strike and any remanent magnetization. The depth is estimated at the source edge from the reciprocal of the local wavenumber.

$$Depth_{(x=0)} = \frac{1}{k_{\max}} \qquad (4)$$

One more advantage of this method is that the interference of anomaly features is reducible, since the method uses the second-order derivatives. The peaks of SPI functions were traced by passing a small 3 by 3 window over the grid data and searching for maxima (Blakely and Simpson, 1986). The traced structures are plotted over a background of the magnetic components. The SPI method was applied to the filtered regional (Fig. 8) and residual (Fig. 9) magnetic component maps. The SPI method could map the linear structures in the both magnetic components with higher resolutions. These structures can be grouped mainly into NE, NW, and NNW directions. The SPI depth estimates from the regional magnetic component (from 1400 to 4200 m) shows deeper values compared to the Euler method. However, these depths agree with that obtained from Euler depths in the relative depths to the structures. Moreover, horizontal dislocation of some deep-seated structures traced from SPI method is obvious in comparison with same structure traced by Euler method. This shift is referred to the methods differences and to the dip of the structure. On the other hand, the SPI depths estimated for the residual magnetic component are close to those obtained from the Euler method. Depth ranges from 400 to 850m was obtained for the near-surface features including dykes, basaltic flow and some ring structures.

DEPTH ESTIMATES OF THE INTRUDED MAGMA

For estimating the depth to the bottom of the magnetic crust (Curie isotherm), which in this case indicates the depth to the intruded high-temperature rocks, we primarily use the azimuthally averaged Fourier spectra of magnetic anomalies (e.g., Spector and Grant, 1970). Analyzing the long wavelength part of the magnetic data can provide information about this depth. This depth represents the depth below which rocks lose their magnetization. We use the slopes of the amplitude spectra to derive the depth to the top (zt) of the magnetic source (e.g., Okubo et al., 1985) and the centroid depths (z0) of the magnetic source. Then, the basal depth of the magnetic source is Zb = 2z0 – zt. Figure 10 shows the amplitude spectrum and the scaled amplitude spectrum of the magnetic data of the Al-Ays area using the centroid method of Okubo et al. (1985).

It is found that a cell area of around 100 km^2 is required to be able to estimate the Curie isotherm depth from spectral estimates using an iterative forward modeling approach of the spectral peak method suggested by Ravat et al. (2007). The depth estimates for shallower Curie isotherms using the selected cell size are stable, and the shape of the spectral peak did not change with an increase in the block size. The deepest magnetic component shows average depth to the top of about (2.3 km) and depth to the bottom (depth to the magma) of about 8.3 km within this area. The estimated depth to the magma show good agreement with the focal depth estimation for the 2009 main shock (9 km) and shallower group of the aftershocks, clustered at two depth intervals between 5 to 10 km and from 15 to 25 km (Al-Zahrani et al., 2012).

CONCLUDING INTERPRETATION

The obtained results (locations and depths) obtained from the analysis methods were compared and integrated to construct the basement tectonic map (Fig. 11). Most of the mapped structures are traced along the solutions aligned and confirmed by both the analysis methods. However, some structures were interpreted following the disruption and discontinuity of the method's solutions. This map shows the deep-seated structures, interpreted from the regional maps, displayed in bold black lines. These deep-seated structures represent the older tectonic features (mainly contacts and faults) trending in NE-SW, NNW-SSE and N-S directions. The depth of these structures ranges from 1000 to 4000 meters.

On the other hand, the near-surface structures were interpreted by the application of the analysis methods to the residual component map. They are mostly dikes, as proved by the Euler method, of different composition and/or magnetic polarization. Accordingly, they are mapped in red coloure for the basic or normally polarized dikes and in blue colour for acidic or reversed polarized dikes. These lineaments show good agreement with the geologically mapped folding systems that may associate with dikes intrusion in the weak zones of the folds (Figs. 2 and 11). The subsurface boundaries of the basaltic flow are shown as hachured polygons, while bold circles show the ring-like volcanic intrusions.

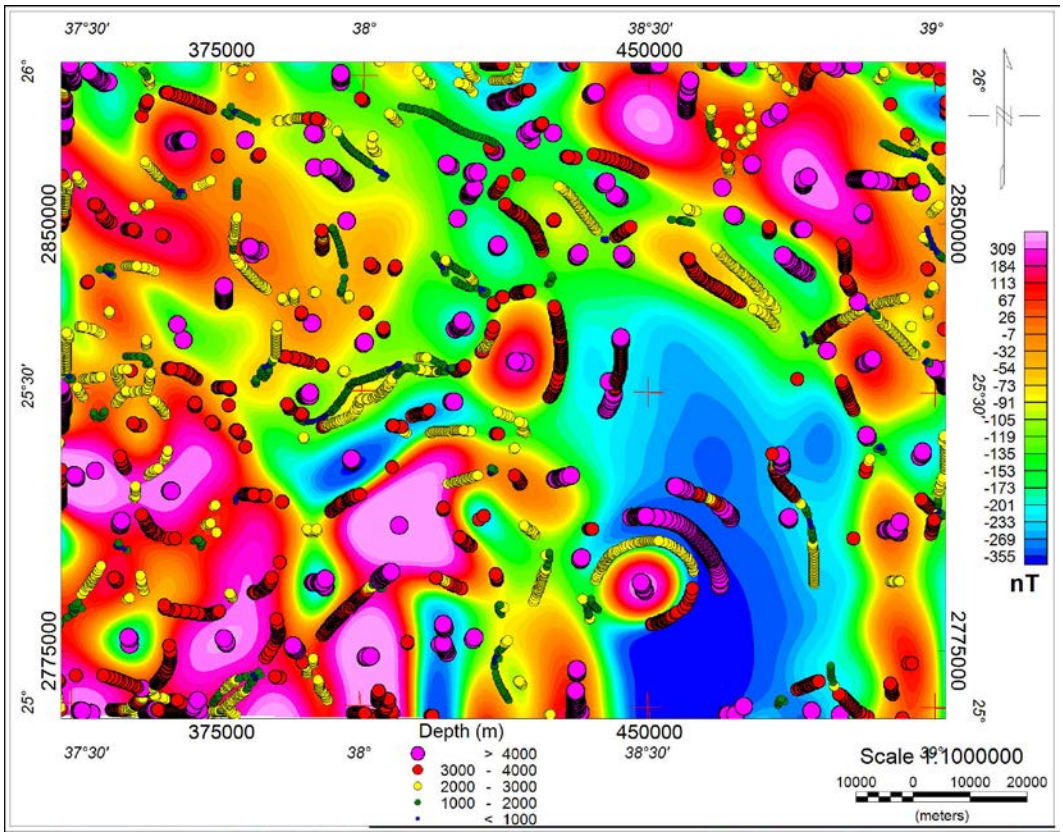

Fig. (8): SPI solutions for the regional magnetic component map (inset as background).

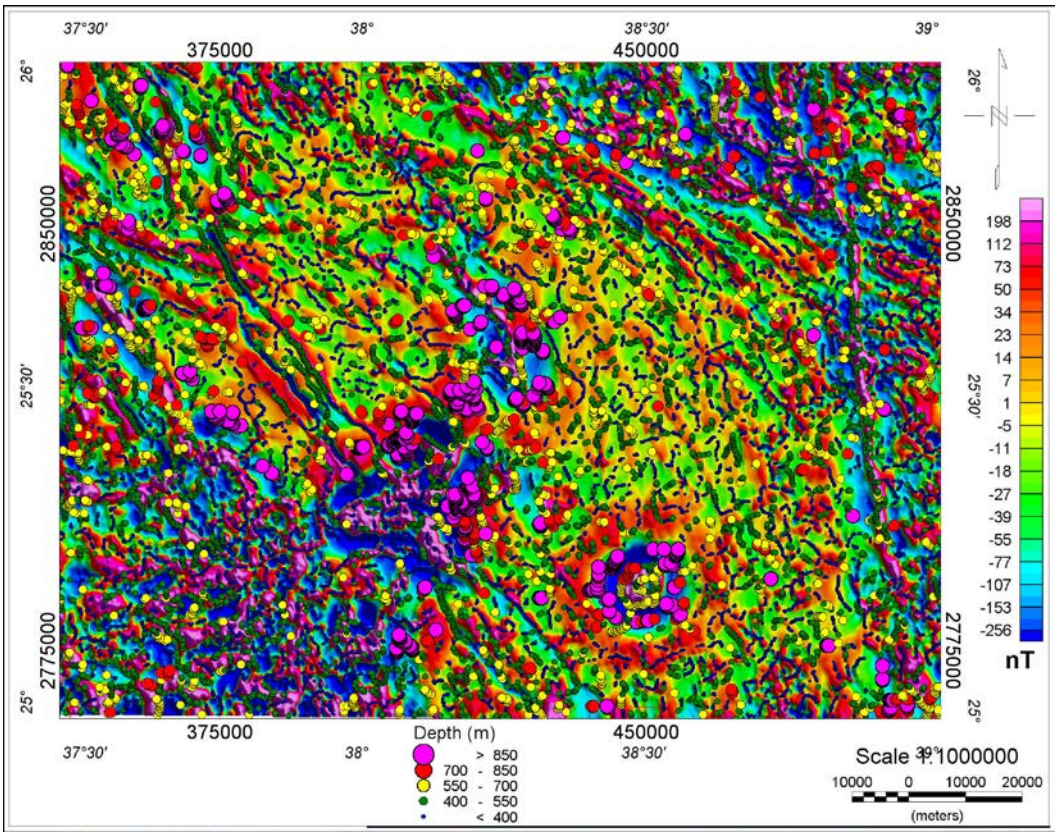

Fig. (9): SPI solutions for the residual magnetic component map.

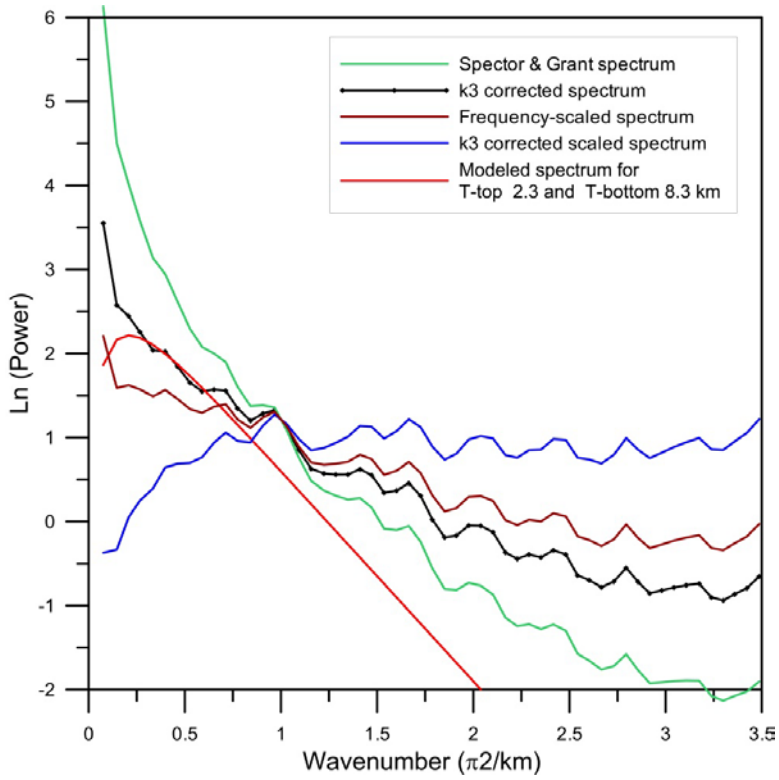

Fig. (10): Spectral analysis of 100 km^2 magnetic window over the seismic active zone using Spector & Grant (green) and Okubo (red) methods as well as the modelled spectra for the obtained depth to the top and bottom (2.3 and 8.3 km).

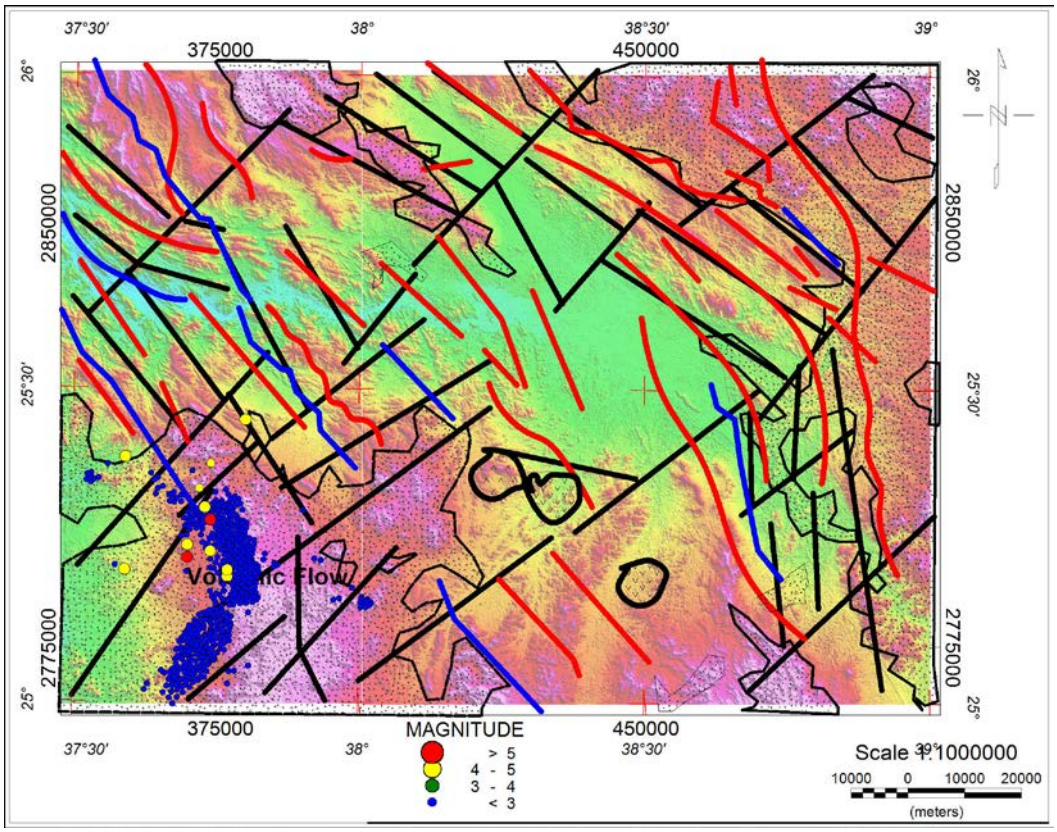

Figure (11): Interpreted structure of the study area superimposed over the topographic map as background. Black lines represent the deep-seated faults, red and blue lines represent the acidic and basic dikes, respectively. The hachured polygon reflects the subsurface basaltic flow areas.

Comparing the interpretation structure, basaltic flow, and depth to the magma at Harte Lunayyir area with the distribution and analysis of the latest seismic events supports the following assumption: the intermediate earthquakes (M ≥4) occurred in association with a fracturing of the basement rocks along one of the NNW-SSE trending faults. This fracturing associated with magmatic intrusion along NE-SW and NNW-SSE trending fault systems resulted in the swarm of the aftershock small earthquakes (M≤3), clustered along these trends. This interpretation agrees with the scenario adopted by Pallister et al., 2010 as interpretation of the recently occurred seismic events.

REFERENCES

Al-Zahrani, H. A., Fnais, M. S., Al-Amri, A. M. and Abdel-Rahman, K. (2012) Review Tectonic Framework of Lunayyir area, northwest Saudi Arabia through aftershock sequence analysis of 19 May, 2009 earthquake and aeromagnetic data, *International Journal of Physical Sciences*, 7(44), 5821-5833.

Anon (1972) The Sea that is really an ocean. *New Sci*. 34:414

Bird, D. (1997) Interpreting magnetic data: Geophysical corner, *EXPLORER*, AAPG and SEG, May, 1997.

Blakely, R.J., and Simpson, R. W. (1986) Approximating edges of source bodies from magnetic or gravity anomalies, *Geophysics*, 51, no.7, 1494-1498.

Elawadi, E., Mogren, S., Ibrahim, E., Batayneh, A., and Al-Bassam, A., (2012) Utilizing potential field data to support delineation of groundwater aquifers in the southern Red Sea coast, Saudi Arabia, Journal of Geophysics and Engineering, 9 , 327–335, doi:10.1088/1742-2132/9/3/327.

Elawadi, E., Zaman, H., Batayneh, A., Mogren, S., Laboun, A., Ghrefat, H., and Zumlot, t., (2013) Structural interpretation of the Ifal Basin in north-western Saudi Arabia from aeromagnetic data: hydrogeological and environmental implications, Exploration Geophysics,doi: http://dx.doi.org/10. 1071 /EG12069.

Geosoft (2005) Oasis Montaj software package. Mapping and Processing System, Ontario, Canada

Kemp, J. (1981) Geologic map of the Wadi Al 'Ays Quadrangle, Sheet No 25 C. Kingdom of Saudi Arabia (scale: 1:250,000). Saudi Arabian Deputy Ministry for Mineral Resources.

Mashael, M. Al-Saud (2008) Structural mapping from high resolution aeromagnetic data in west central Arabian Shield, Saudi Arabia using normalized derivatives, *Arab J. Geosciences*, 1, 129–136.

Nehlig, P., Genna, A., Asfirane, F., Dubreuil, N., Guerrot, C., Eberlé, J.M., Kluyver, H.M, Lasserre, J.L., Le Goff, E , Nicol, N, Salpeteur, N., Shanti, M., Thiéblemont, D., and Truffert, C (2002) A review of the Pan-African evolution of the Arabian Shield, *GeoArabia*, 7, No. 1, 103-124, (Gulf PetroLink, Bahrain).

Okubo, Y., Graf, R.J., Hansen, R.O., Ogawa, K., Tsu, H., (1985) Curie-point depths of the island of Kyushu and surrounding areas, Japan. *Geophysics* 50 (3), 481–494.

Pallister, J., S., McCausland, W. A., Jónsson, S., Lu, Z., Zahran, H., M., El Hadidy, S., Aburukbah, A., Stewart, I., Lundgren, P., R., White, R., A., and Moufti, M., R., (2010) Broad accommodation of rift-related extension recorded by dyke intrusion in Saudi Arabia, Nature Geoscience, 3, 705-712, DOI: 10.1038/NGEO966.

Ravat, D., Pignatelli, A., Nicolosi, I., Chiappini, M., (2007) A study of spectral methods of estimating the depth to the bottom of magnetic sources from near-surface magnetic anomaly data. *Geophysical Journal International*, 169 (2), 421–434.

Reid, A.B., Allsop, J. M., Granser, H., Millet, A. J., and Somerton, I. W. (1990) Magnetic interpretation in three dimensions using Euler deconvolution, *Geophysics*, 55, 80-91.

Rose, D.A; Whitmarsh, R.B; Ali, S.A.; Boudreaux, J.E; Coleman, R.G; Fleisher, R.L.; Girdler, R.; Manheim, F.; Matter, A.; Nigrini C.; Stoffers, P. and Supko, P.R. (1973) Red Sea, drilling. Science, 179: 377-380.

Smith, R. S., Thurston, J. B., Dai, Ting-Fan, and MacLeod, I. N. (1998) ISPI - the improved source parameter imaging method, *Geophysical Prospecting*, 46, 141-151.

Spector, A., Grant, F.S., (1970) Statistical models for interpreting aeromagnetic data, *Geophysics*, 35, 293–302.

Thompson, D. T. (1982) "EULDPH" A new technique for making computer-assisted depth estimates from magnetic data, *Geophysics*, 47, 31-37.

Thurston, J. B. and Smith, R. S. (1997) Automatic conversion of magnetic data to depth, dip, susceptibility contrast using the SPI^{TM} method, *Geophysics*, 62, 807–813.